Journal of Japan Association for Earthquake Engineering, Vol. 25, No. 13, 2025
[Technical Paper (Translated Paper)]

GENERATION MECHANISM OF V_{non}, THE APPARENT RESIDUAL VERTICAL VELOCITY IN STRONG MOTION RECORDS

Atsushi NOZU[1]

[1] Member, Dr. Eng., Senior Director of Research, Port and Airport Research Institute,
Kanagawa, Japan, nozu@p.mpat.go.jp

ABSTRACT: In previous studies, it was suggested that integrating the vertical component of strong acceleration records in time domain often yields a residual velocity, which is always negative. This study proposes a generation mechanism of this residual velocity V_{non}; at the moment of the action of a horizontal inertia force, the sensor is tentatively tilted in that direction and the horizontal inertia force multiplied by $\sin\theta$ is felt by the vertical sensor, where θ is the tilt angle. The tilt of the sensor can be either due to the shear deformation of the ground or the tilt of the house. The apparent residual velocity generated by this mechanism is always negative. It was shown for the K-NET records for which the effect of the housing is small that the proposed mechanism can readily explain the order of magnitude of the observed V_{non} values.

Keywords: *Strong motion record, Vertical motion,* V_{non}*, Shear deformation, Tilt,* $G\text{–}\gamma$ *curve*

1. INTRODUCTION

There have been interesting reports[1)–3)] that the vertical components of recently-obtained large-amplitude accelerograms often result in a negative residual velocity once they are integrated in time domain. One of the reports[3)] shows that there are 26 records with a residual velocity exceeding 5 cm/s. Among them are records observed by various observation networks such as K-NET[4)], KiK-net[4)] and the JMA network, and records of various types of earthquakes such as crustal, interplate and intraslab earthquakes. The hypocentral distance also ranges from 11–319 km. The author of this article also integrated those records in time domain and confirmed that they result in negative residual velocities, with absolute values as large as in the previous report[3)].

The previous reports[1)–3)] also investigated the generation mechanism of this negative residual velocity. Although the previous reports did not give a complete physical and quantitative explanation of the phenomena, the reports did suggest the effects of soil dilatancy because of the following reasons. 1. The predominant frequencies for the vertical components were twice as large as those for the horizontal components for the records, which is symptomatic of soil dilatancy in which the soil changes its volume under shear[5), 6)]. 2. This tendency of predominant frequency was not observed for the record at KiK-net IWTH25 during the 2008 Iwate-Miyagi Nairiku earthquake for which no evident residual velocity was observed in spite of the large amplitude. The previous reports[1), 3)] also suggested that the negative residual velocity V_{non} can be used to detect the nonlinear amplification of vertical ground motions.

The author of this article also agrees that these records were somehow affected by soil nonlinearity referring to the characteristics of the records mentioned above, and does not disagree with the involvement of soil dilatancy. However, it should be emphasized here that the residual values appear in the velocity waveforms rather than the displacement waveforms. If this showed the actual behavior of the ground, the results would indicate that the ground continued subsiding even after the ground shaking with a velocity greater than 5 cm/s, which would then result in a subsidence of 3 m in one minute, which is unrealistic. Even if soil dilatancy is involved in the process, the residual velocity is not representing the actual subsidence due to soil dilatancy. Thus, the residual velocity V_{non} is apparent. This study investigated the generation mechanism of V_{non} with a premise that it is an apparent value.

One interesting feature of V_{non} is that the residual velocity is always negative (as long as the upward acceleration is measured as positive). In general, in the case of small-amplitude accelerograms, it is not surprising that integrated velocities are susceptible to errors dur to electronic noise in low frequencies. However, if electronic noise is causing the residual velocity, it could be either positive or negative. Therefore, electronic noise is excluded from the candidate mechanisms. Another interesting feature of V_{non} is that it is widely observed as mentioned above. This indicates that the mechanism leading to the generation of V_{non} is not a rare special phenomenon but a widely-occurring phenomenon. Thus, the generation mechanism of V_{non} should satisfy the following two conditions. 1. The mechanism should always lead to a negative residual velocity. 2. The mechanism is a widely-occurring phenomenon.

This study newly proposes a generation mechanism of V_{non} that satisfies the above two conditions; at the moment of the action of a horizontal inertia force, the sensor is tentatively tilted in that direction and the horizontal inertia force multiplied by $\sin\theta$ is felt by the vertical sensor, where θ is the tilt angle. The tilt of the sensor can be either due to the shear deformation of the ground in the case of a sensor buried in the ground or attached to a foundation which is buried in the ground, or due to the tilt of the house in the case of a sensor installed in a house. Although another mechanism can also be considered in which the gravitational acceleration felt by the vertical sensor is tentatively decreased due to the tilt of the sensor, the effect of this mechanism is limited as the gravitational acceleration is multiplied by $(1-\cos\theta)$ in this mechanism as pointed out in the previous reports[2), 3)] (this point will also be confirmed in this article). The mechanism in which the horizontal inertia force is partly felt by the vertical sensor has not been considered in previous studies and therefore it is worthwhile investigating it in this study. This mechanism satisfies the above two conditions because the phenomenon can widely occur and also the apparent residual velocity caused by this mechanism is always negative.

It is important to investigate whether the proposed mechanism can explain the order of magnitude of the observed V_{non} values. Therefore, in this study, the V_{non} values were calculated based on the proposed mechanism for the cases in which the tilt of the sensor is caused by the shear deformation of the ground.

In the ensuing sections, the generation mechanism of V_{non} will be explained in 2. The calculation method of the V_{non} values based on the proposed mechanism will be explained in 3. The calculation results will be presented in 4. Discussion will be made in 5. Conclusions will be described in 6.

2. THE GENERATION MECHANISM OF V_{non} PROPOSED IN THIS STUDY

In this section, the generation mechanism of V_{non} will be explained, mainly focusing on the cases in which the tilt of the sensor is caused by the shear deformation of the ground. Figure 1 shows the near-surface ground repeatedly subject to positive and negative horizontal accelerations. Figure 1 (a) shows the situation in which the ground displacement to the left is maximized, with the horizontal inertia force pointing left. At this moment, due to the action of the shear force, the ground will be deformed to form a parallelogram as shown in Fig. 1 (a). If we assume that the sensor is buried in the ground and follows the shear deformation of the ground, the sensor will be inclined and the horizontal inertia force multiplied by $\sin\theta$ will be felt by the vertical sensor, where θ is the tilt angle. This force will inevitably be pointing upward and conceived by the vertical sensor as resulting from a downward acceleration. Integrating this acceleration yields a residual negative velocity. Figure 1 (c) shows the situation in which the ground displacement to the right is maximized. Due to symmetry, the force felt by the vertical sensor will again be pointing upward and conceived by the vertical sensor as resulting from a downward acceleration. On the other hand, in the situations shown in Fig. 1 (a) and (c), the gravitational acceleration felt by the vertical sensor is tentatively decreased due to the tilt of the sensor. However, its effect is limited as the gravitational acceleration is multiplied by $(1-\cos\theta)$ in this mechanism as pointed out in the previous reports[2), 3)] (this point will also be confirmed in this article).

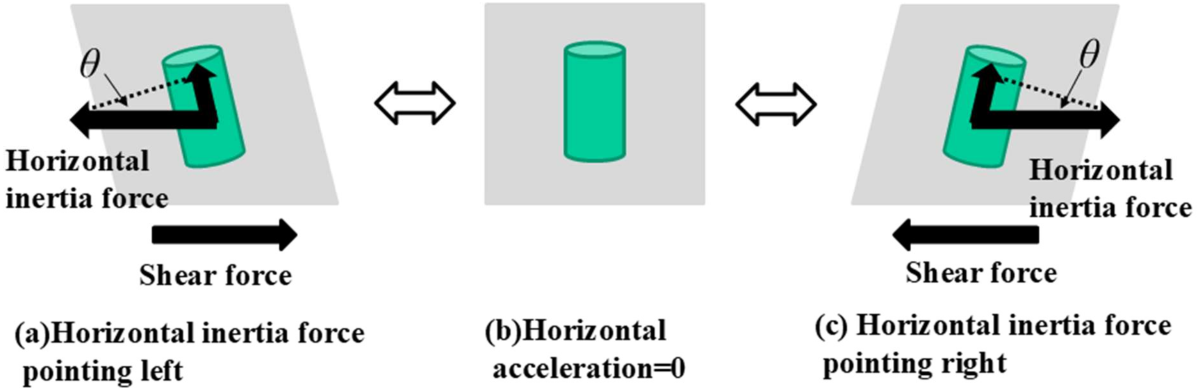

Fig. 1 The generation mechanism of V_{non} proposed in this study

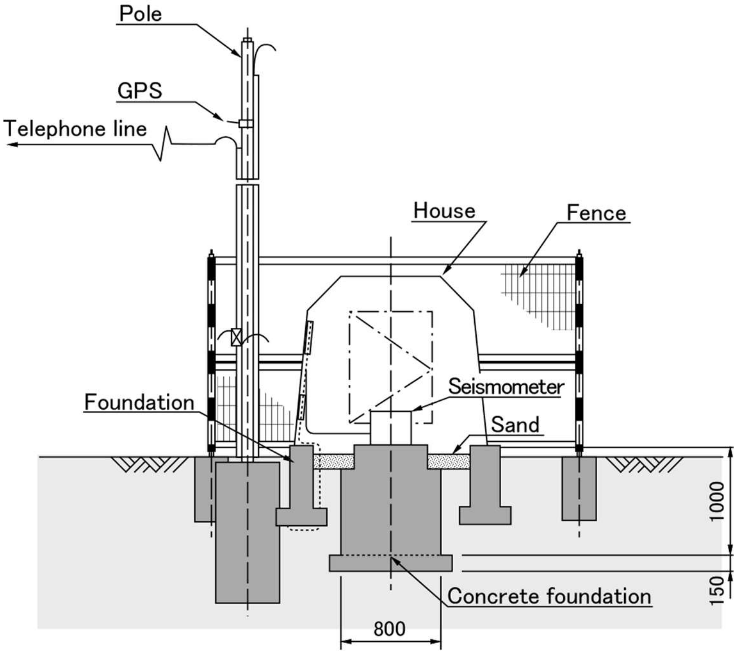

Fig. 2 Typical observation station of K-NET (after Fig. 2 of Aoi et al.[7)]; unit: mm)

In the above explanation, it was assumed that the sensor is buried in the ground to explain the generation mechanism of V_{non}. Alternatively, if the sensor is attached to a foundation which is buried in the ground as typically seen in K-NET stations (Fig. 2), if the foundation follows the shear deformation of the ground, the tilt of the sensor will generate V_{non}. Even if the sensor is installed in a house, if the tilt of the house is in phase with the action of the horizontal inertia force as shown in Fig.

1, the same mechanism will generate V_{non}.

Because of the simplicity of the proposed mechanism, the phenomenon can widely occur and the mechanism is advantageous to explain the fact that V_{non} has been observed under various circumstances. In addition, the mechanism always results in a negative residual velocity.

3. CALCULATION MEHOD OF V_{non} BASED ON THE PROPOSED MECHANISM

In the following, it will be investigated if the proposed mechanism can explain the order of magnitude of the observed V_{non} values. There are K-NET, KiK-net and JMA records with the V_{non} values exceeding 5 cm/s[3]. Among them, the surface sensors of KiK-net are installed in houses according to Aoi et al.[7] which makes it difficult to evaluate the tilt of the sensors without information on the size, etc. of the individual houses. In addition, the author does not have detailed information on the installation conditions of the JMA sensors. On the other hand, for the K-NET stations, the sensors are either fixed on a concrete foundation buried in the ground (Fig. 2) or fixed in a pit inside a concrete foundation buried in the ground for cold regions[8], except for the stations that existed prior to the establishment of K-NET and the ocean-bottom stations (Aoi, personal communication). The sensor foundation is independent from the foundation of the house, which makes the effect of the house negligible for the K-NET stations. Therefore, in the following, the focus is on the K-NET records. There are 16 K-NET records with the V_{non} values exceeding 5 cm/s as show in Table 1. These records will be the target of the following analyses.

The calculation method of V_{non} based on the proposed mechanism is shown below. Because the foundation shown in Fig. 2 is 1 m high, the shear strain of the ground at a depth of $z = 0.5$ m is taken as a representative value of the shear strain and assumed to determine the tilt of the foundation. Assuming that the ground acceleration is uniform for the shallowest layer with a thickness of 0.5 m, the following relation can be derived among the peak ground acceleration a_{max}, the peak shear stress τ_{max} at $z = 0.5$ m and the density ρ:

$$\tau_{max} = \rho z a_{max}. \tag{1}$$

The relation between the peak shear stress and the peak shear strain γ_{max} is given as follows:

$$\tau_{max} = G\gamma_{max} \tag{2}$$

where G is the shear modulus during strong shaking. One the other hand, the relation between the linear shear modulus and the linear shear wave velocity is given as follows:

$$G_0 = \rho {\beta_0}^2 \tag{3}$$

Equations (1)–(3) yields the following relation:

$$(G/G_0) \cdot \gamma_{max} = z a_{max}/{\beta_0}^2 \tag{4}$$

The right-hand side of Eq. (4) can be determined from the observation record and the soil data. Therefore, Eq. (4) represents a hyperbola in the G/G_0–γ plane. Although this equation uses the shear wave velocity at z =0.5 m, due to the limited resolution of the published soil data, the shear wave velocity at the shallowest layer (Table 1) will be used in the following analyses unless mentioned otherwise. The thickness of the shallowest layer in Table 1 shows the thickness for which the same shear wave velocity is assigned in the data. For the same reason, the soil type at the shallowest layer (Table 1) will be used in the following analyses. The thickness of the shallowest layer in Table 1 does not show the thickness for which the same soil type is assigned in the data.

Table 1 K-NET records with the V_{non} values exceeding 5 cm/s[3)]

Station code	Year, month, day	Type	$\mathrm{M_J}$	Hypocentral distance (km)	V_{non}[3)] (cm/s)	Peak ground acceleration (cm/s^2)[3)]			V_S* (m/s)	Thickness* (m)	Soil type*
						EW	NS	UD			
HKD086**	20030926	Plate boundary	8.0	127	76.7	801	728	271	120	1	Gravel
MYG004**	20110311	Plate boundary	9.0	177	33.5	1269	2699	1880	100	1	Clay
IBR013	20110311	Plate boundary	9.0	303	19.2	1072	1352	811	100	4	Fill soil
TCG009	20110311	Plate boundary	9.0	319	17.4	1185	1017	493	100	4	Fill soil
IBR003	20110311	Plate boundary	9.0	259	13.9	1185	1599	1166	100	3	Fill soil
FKS016	20110311	Plate boundary	9.0	261	13.8	949	1295	441	50	1	Fill soil
HKD127	20180906	Crustal	6.7	45	13.4	907	1003	1591	130	2	Sand
HKD100	20030926	Plate boundary	8.0	94	12.6	970	809	461	100	2	Volcanic clay
NIG019**	20041023	Crustal	6.8	15	12.6	1314	1144	820	100	3	Fill soil
TCG014	20110311	Plate boundary	9.0	295	9.4	1205	710	494	225	3	Volcanic clay
MYG004**	20110407	Intraslab	7.2	118	9.0	886	1241	476	100	1	Clay
MYG011**	20030526	Intraslab	7.0	92	6.5	1114	1101	825	130	1	Fill soil
MYG002	20110311	Plate boundary	9.0	139	6.1	659	641	362	140	1	Sand
IWT009	20110311	Plate boundary	9.0	164	5.2	512	570	299	130	2	Fill soil
HKD066	20030926	Plate boundary	8.0	230	5.2	492	430	157	60	3	Fill soil
IBR013	20110311 B***	Plate boundary	7.6	82	5.0	924	556	347	100	4	Fill soil

* V_S, thickness, and soil type correspond to the shallowest layer.

** For the records obtained at a station before migration, the soil data corresponds to the station before the migration.

*** 20110311B shows the largest aftershock of the 2011 Tohoku earthquake.

As an example, the curve in Eq. (4) was obtained from the NS component accelerogram of the record at MYG004 during the March 11, 2011, Tohoku earthquake, which produced one of the largest V_{non} values, and plotted in Fig. 3. By finding the intersection of this curve and a G/G_0–γ curve obtained from laboratory tests, G/G_0 and γ can be determined. Although it is a common practice to use the effective strain $\gamma_{eff} = 0.65\gamma_{max}$ for a G/G_0–γ curve, γ_{max} will be directly used in this study because the shear modulus at the moment of the peak acceleration is concerned. Among various G/G_0–γ curves, the curves proposed by Imazu and Fukutake[9), 10)] for various soils will be used, because Imazu and Fukutake showed not only the average curves but also the range of the curves and, by showing that the observed V_{non} values can be explained within the possible range of the G/G_0–γ curves, it can be shown that the proposed generation mechanism of V_{non} is plausible. Figure 3 shows the Imazu-Fukutake G/G_0–γ curves for clay, because the shallowest layer at MYG004 was a clay layer before the migration of the station. Using different G/G_0–γ curves results in different intersections with the curve in Eq. (4), i.e., different G/G_0 and γ values, and consequently results in different V_{non} values. It should be noted that, in the Imazu-Fukutake curves, $\mu+\sigma$ corresponds to a smaller stiffness, and $\mu-\sigma$ corresponds to a larger stiffness.

Once G/G_0 is determined, it will be applied to the entire time history. This aspect of analyses is similar to equivalent linear analyses. For a given horizontal acceleration time history $a(t)$, the time history of shear stress at z =0.5 m is given by

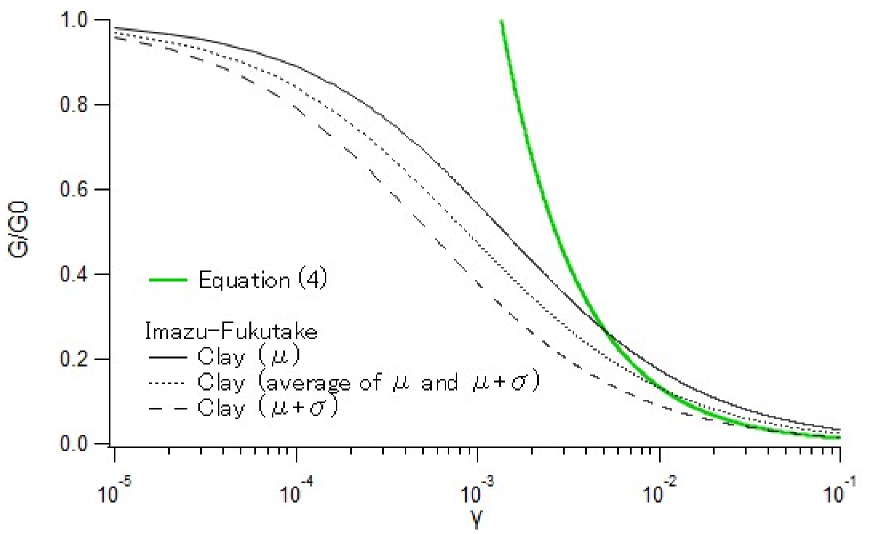

Fig. 3 Curve in Eq. (4) obtained from the NS component accelerogram of the record at MYG004 during the March 11, 2011, Tohoku earthquake (green line). The Imazu-Fukutake G/G_0–γ curves for clay[9), 10)] are also plotted (black lines).

$$\tau(t) = -\rho z a(t) \tag{5}$$

and the time history of shear strain at z =0.5 m is given by

$$\gamma(t) = \frac{\tau(t)}{G} = -\frac{z}{(G/G_0){\beta_0}^2} a(t) \tag{6}$$

Equation (6) also represents the time history of the tilt of the foundation, and the time history of the tilt of the sensor fixed to the foundation. In other words, $\sin\theta$ can be approximated by $\gamma(t)$. Then, the horizontal acceleration multiplied by $\gamma(t)$ will be felt by the vertical sensor as a downward acceleration. The time history of the apparent acceleration $\tilde{a}_v(t)$ will be

$$\tilde{a}_v(t) = a(t)\gamma(t) = -\frac{z}{(G/G_0){\beta_0}^2} a(t)^2 \tag{7}$$

and the time history of the apparent velocity $\tilde{v}_v(t)$ will be

$$\tilde{v}_v(t) = -\frac{z}{(G/G_0){\beta_0}^2} \int_0^t a(t')^2 dt' \tag{8}$$

The tilt of the sensor can occur in both horizontal directions. Thus, $\tilde{v}_v(t)$ calculated for two horizontal directions will be summed. The residual value of $\tilde{v}_v(t)$ after the summation will be adopted as V_{non}. This method was applied to all the records in Tabel 1. The trapezoidal rule was used for the integration in Eq. (8).

4. CALCULATION RESULTS OF V_{non} BASED ON THE PROPOSED MECHANISM

The two horizontal accelerograms of the record at MYG004 during the March 11, 2011, Tohoku earthquake, which produced one of the largest V_{non} values, were baseline corrected using the average accelerations in 0–5 s and integrated in time domain with the trapezoidal rule. Each of the obtained velocity waveforms can be approximated by two straight lines intersecting at the significant part of the time history as shown in Fig. 4. The bend in the velocity waveform indicates the involvement of a

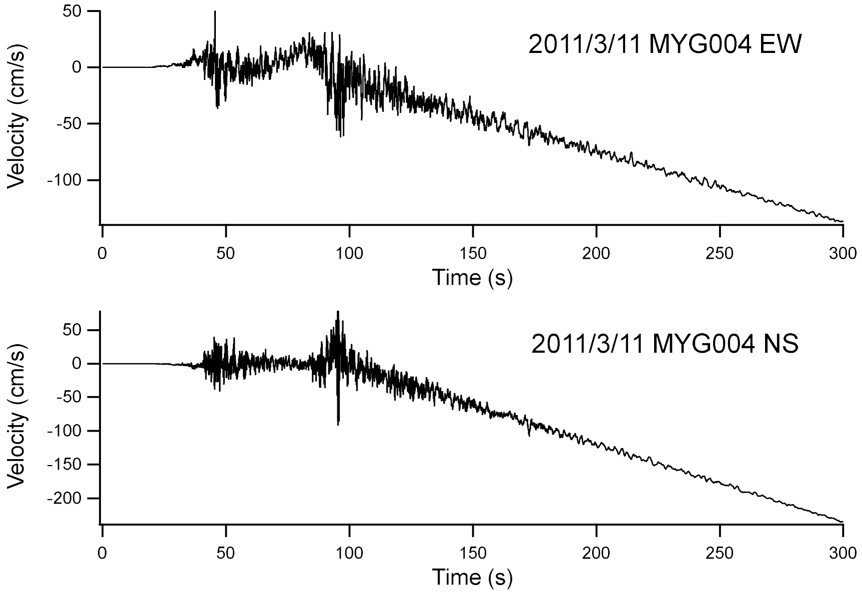

Fig. 4 Velocity waveforms obtained by baseline correcting and integrating in time domain the two horizontal accelerograms of the March 11, 2011, Tohoku earthquake at MYG004

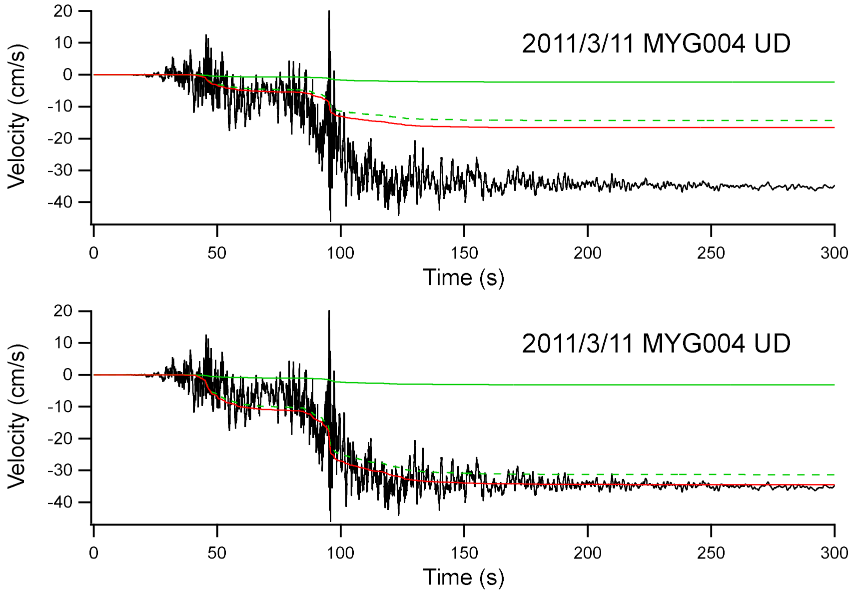

Fig. 5 Velocity waveform obtained by baseline correcting and integrating in time domain the vertical accelerogram of the March 11, 2011, Tohoku earthquake at MYG004 (black lines, common in top and bottom panels) and the time histories of the apparent velocity $\tilde{v}_v(t)$ considering the tilt of the sensor. The Imazu-Fukutake G/G_0–γ curves for clay for μ (top) and the average of μ and μ+σ (bottom) were used. The apparent velocity was calculated from the EW (solid green line) and NS (dashed green line) components. The red line shows the summation.

step-like signal in the accelerogram. This could be due to the residual tilt of the sensor during strong shaking11). This phenomenon observed in the horizontal accelerograms will not be discussed hereinafter, because this is not the topic of this article. On the other hand, the vertical accelerogram of the same record was baseline corrected and integrated in time domain, in the similar way as the horizontal components, and plotted in Fig. 5. The tendency is quite different from the horizontal components; the velocity does not increase or decrease linearly but has a residual value. This is the V_{non} value found in the previous reports1)–3). In the following, it will be investigated if the proposed mechanism can explain this residual value. Throughout this study, the baseline correction of the accelerograms will be conducted using the average accelerations in 0–5 s. As an exception to this, the accelerograms of the largest aftershock of the 2011 Tohoku earthquake at IBR013 were baseline corrected using the average accelerations in 50–100 s, because the initial part was contaminated by signals from another event.

Figure 5 shows the time histories of the apparent velocity $\tilde{v}_v(t)$ considering the tilt of the sensor based on the method described in 3. The Imazu-Fukutake G/G_0–γ curves for clay for μ (top) and the average of μ and μ+σ (bottom) were used. The apparent velocity was calculated from the EW (solid green line) and NS (dashed green line) components based on Eqs. (7) and (8). The red line shows the summation, which is likely to be observed. When the G/G_0–γ curve for μ was used, approximately 50% of the observed V_{non} value was reproduced. When the G/G_0–γ curve for the average of μ and μ+σ was used, the observed V_{non} value was almost reproduced. The observed accumulation of the apparent velocity with time was also reproduced. Therefore, the proposed mechanism in which the horizontal inertia force is partly felt by the tilted vertical sensor is plausible as the generation mechanism of V_{non}.

For other records shown in Table 1, the time histories of the apparent velocity $\tilde{v}_v(t)$ were calculated considering the tilt of the sensor based on the same method and compared with the velocity waveform integrated from the vertical accelerogram in time domain. The results are summarized in Table 2.

Figure 6 shows the results for the record of the September 26, 2003, Tokachi-oki earthquake at HKD086. The Imazu-Fukutake G/G_0–γ curves for gravel were used because the shallowest layer at HKD086 was a gravel layer before the migration of the station. The observed V_{non} value was not successfully reproduced in this case. The possible cause of this result will be discussed later. Figure 7 shows the results for the record of the March 11, 2011, Tohoku earthquake at IBR013. The shallowest layer at IBR013 was categorized as fill soil with no further detailed information. If we use the Imazu-Fukutake G/G_0–γ curves for sand, the observed V_{non} value was successfully reproduced with the curve for μ. Figure 8 shows the results for the record of the March 11, 2011, Tohoku earthquake at TCG009. The shallowest layer at TCG009 was categorized as fill soil with no further detailed information. If we use the Imazu-Fukutake G/G_0–γ curves for sand, the observed V_{non} value was underestimated for the curve for μ and overestimated for the curve for the average of μ and μ+σ. It will be reasonable to postulate that the actual behavior was between them. Figure 9 shows the results for the record of the March 11, 2011, Tohoku earthquake at IBR003. The shallowest layer at IBR003 was categorized as fill soil with no further detailed information. If we use the Imazu-Fukutake G/G_0–γ curves for sand, the observed V_{non} value was underestimated for the curve for the average of μ and μ-σ and overestimated for the curve for μ. It will be reasonable to postulate that the actual behavior was between them. Figure 10 shows the results for the record of the March 11, 2011, Tohoku earthquake at FKS016. The shallowest layer at FKS016 was categorized as fill soil with no further detailed information. Because the shear wave velocity of the shallowest layer is as small as 50 m/s and the hyperbola of Eq. (4) is located in the top-right of the G/G_0–γ plane, if we use the Imazu-Fukutake G/G_0–γ curves for sand, the intersection cannot be found. Therefore, the Imazu-Fukutake G/G_0–γ curves for clay were used. The observed V_{non} value was successfully reproduced with the curve for the average of μ and μ-σ. Figure 11 shows the results for the record of the September 6, 2018, Hokkaido Eastern Iburi earthquake at HKD127. The Imazu-Fukutake $G/G_0-\gamma$ curves for sand were used because the shallowest layer at HKD127 was a sand layer. The observed V_{non} value was not successfully reproduced in this case. The possible cause of this result will be discussed later. Figure 12 shows the results for the record of the September 26, 2003, Tokachi-oki earthquake at HKD100. The Imazu-Fukutake G/G_0–γ curves for clay were used because the shallowest layer at HKD100 was a volcanic clay layer. The observed V_{non} value was not successfully reproduced in this case. The possible cause of this result will be discussed later. Figure 13 shows the results for the record of the October 23, 2004, Mid Niigata Prefecture earthquake at NIG019. The shallowest layer at NIG019 before the migration of the station was categorized as fill soil with no further detailed information. If we use the Imazu-Fukutake

Table 2 Reproducibility of the V_{non} values based on the proposed mechanism

Station code	Year, month, day	V_{non}3) (cm/s)	Soil type*	Reproducibility of V_{non}****	G/G_0–γ curve that can reproduce V_{non}	Possible cause of unsatisfactory reproduction of V_{non}
HKD086**	20030926	76.7	Gravel	Bad	—	Liquefaction of the backfill soil and the tilt of the foundation
MYG004**	20110311	33.5	Clay	Very good	Clay, the average of μ and μ+σ	
IBR013	20110311	19.2	Fill soil	Very good	Sand, μ	
TCG009	20110311	17.4	Fill soil	Very good	Sand, between μ and the average of μ and μ+σ	
IBR003	20110311	13.9	Fill soil	Very good	Sand, between μ and the average of μ and μ-σ	
FKS016	20110311	13.8	Fill soil	Very good	Clay, the average of μ and μ-σ	
HKD127	20180906	13.4	Sand	Good	Sand, μ+σ	
HKD100	20030926	12.6	Volcanic clay	Bad	—	Excess pore water pressure generation in the unsaturated volcanic clay
NIG019**	20041023	12.6	Fill soil	Very good	Sand, the average of μ and μ+σ	
TCG014	20110311	9.4	Volcanic clay	Bad	—	Excess pore water pressure generation in the unsaturated volcanic clay
MYG004**	20110407	9.0	Clay	Very good	Clay, μ+σ	
MYG011**	20030526	6.5	Fill soil	Very good	Sand, μ+σ	
MYG002	20110311	6.1	Sand	Bad	—	Upward propagation of the excess pore water pressure
IWT009	20110311	5.2	Fill soil	Good	Sand, μ+σ	
HKD066	20030926	5.2	Fill soil	Very good	Sand, μ	
IBR013	20110311 B***	5.0	Fill soil	Very good	Sand, the average of μ and μ+σ	

* Soil type corresponds to the shallowest layer.

** For the records obtained at a station before migration, the soil data corresponds to the station before the migration.

*** 20110311B shows the largest aftershock of the 2011 Tohoku earthquake.

**** 'Very good' means reproducible with the published V_S for the shallowest layer. 'Good' means reproducible with the depth dependent V_S.

G/G_0–γ curves for sand, the observed V_{non} value was successfully reproduced with the curve for the average of μ and μ+σ. Figure 14 shows the results for the record of the March 11, 2011, Tohoku earthquake at TCG014. The Imazu-Fukutake G/G_0–γ curves for clay were used because the shallowest layer at TCG014 was a volcanic clay layer. The observed V_{non} value was not successfully reproduced in this case. The possible cause of this result will be discussed later. Figure 15 shows the results for the record of the April 7, 2011, intraslab earthquake at MYG004. The Imazu-Fukutake G/G_0–γ curves for clay were used because the shallowest layer at MYG004 before the migration of the station was a clay layer. The observed V_{non} value was successfully reproduced with the curve for μ+σ. Figure 16 shows the results for the record of the May 26, 2003, intraslab earthquake at MYG011. The shallowest layer at MYG011 before the migration of the station was categorized as fill soil with no further detailed information. If we use the Imazu-Fukutake G/G_0–γ curves for sand, the observed V_{non} value was successfully reproduced with the curve for μ+σ. Figure 17 shows the results for the record of the March 11, 2011, Tohoku earthquake at MYG002. The Imazu-Fukutake G/G_0–γ curves for sand were used because the shallowest layer at MYG002 was a sand layer. The observed V_{non} value was not successfully reproduced in this case. The possible cause of this result will be discussed later. Figure 18

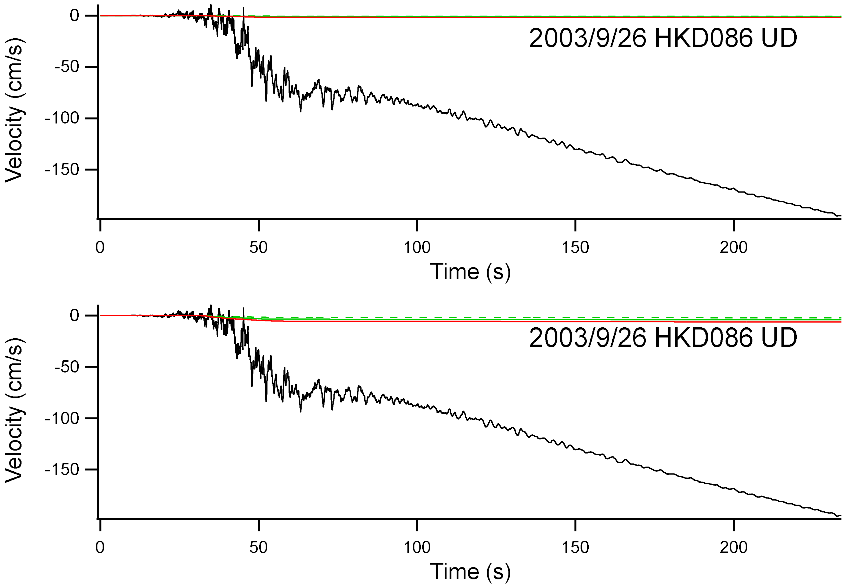

Fig. 6 Velocity waveform obtained by baseline correcting and integrating in time domain the vertical accelerogram of the September 26, 2003, Tokachi-oki earthquake at HKD086 (black lines, common in top and bottom panels) and the time histories of the apparent velocity $\tilde{v}_v(t)$ considering the tilt of the sensor. The Imazu-Fukutake G/G_0–γ curves for gravel for μ (top) and the average of μ and μ+σ (bottom) were used. The apparent velocity was calculated from the EW (solid green line) and NS (dashed green line) components. The red line shows the summation.

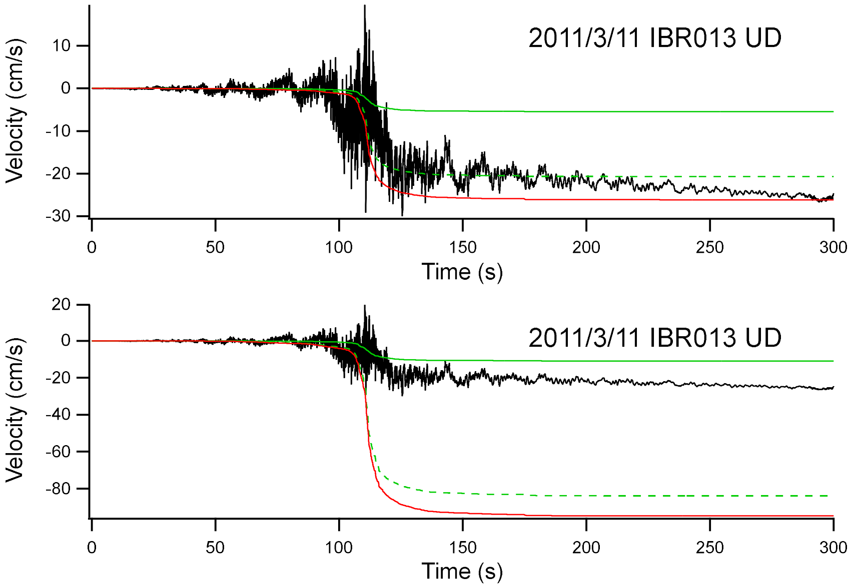

Fig. 7 Velocity waveform obtained by baseline correcting and integrating in time domain the vertical accelerogram of the March 11, 2011, Tohoku earthquake at IBR013 (black lines, common in top and bottom panels) and the time histories of the apparent velocity $\tilde{v}_v(t)$ considering the tilt of the sensor. The Imazu-Fukutake G/G_0–γ curves for sand for μ (top) and the average of μ and μ+σ (bottom) were used. The apparent velocity was calculated from the EW (solid green line) and NS (dashed green line) components. The red line shows the summation.

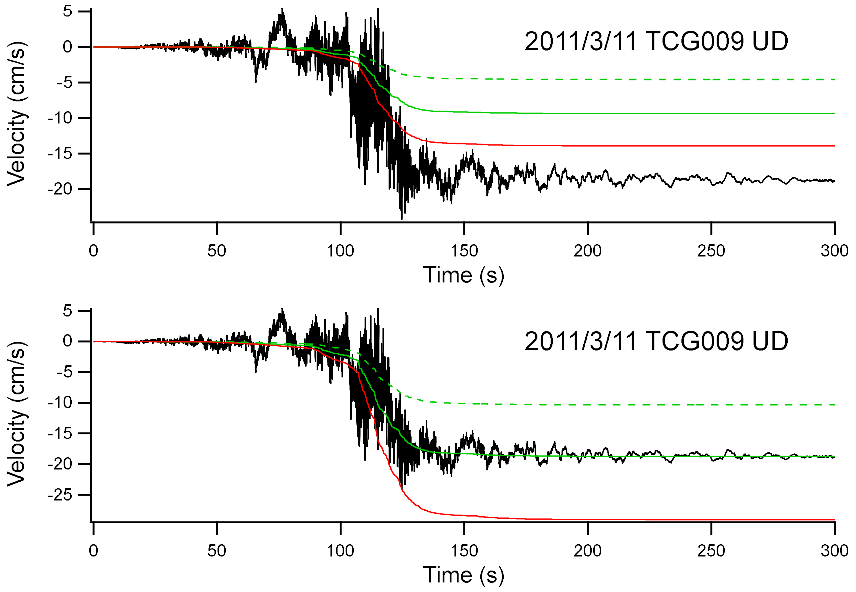

Fig. 8 Velocity waveform obtained by baseline correcting and integrating in time domain the vertical accelerogram of the March 11, 2011, Tohoku earthquake at TCG009 (black lines, common in top and bottom panels) and the time histories of the apparent velocity $\tilde{v}_v(t)$ considering the tilt of the sensor. The Imazu-Fukutake G/G_0–γ curves for sand for μ (top) and the average of μ and μ+σ (bottom) were used. The apparent velocity was calculated from the EW (solid green line) and NS (dashed green line) components. The red line shows the summation.

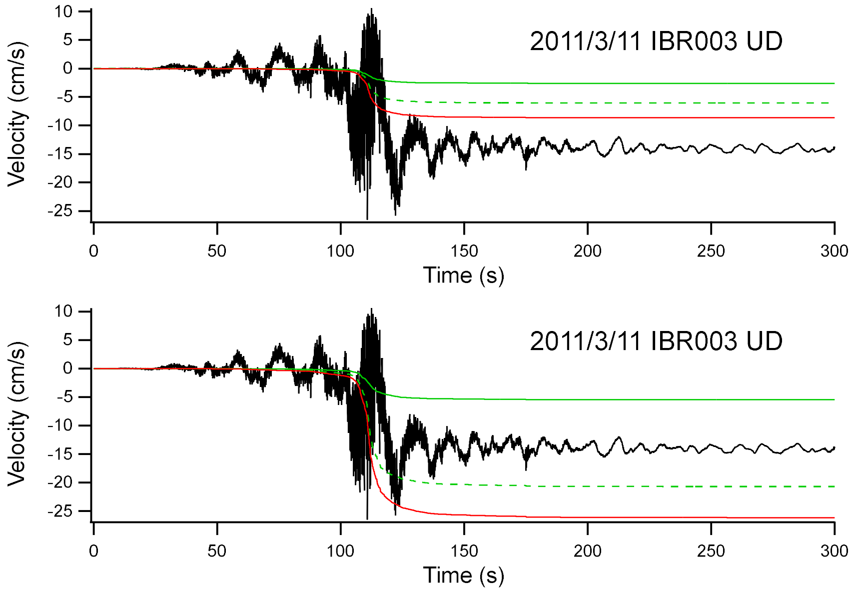

Fig. 9 Velocity waveform obtained by baseline correcting and integrating in time domain the vertical accelerogram of the March 11, 2011, Tohoku earthquake at IBR003 (black lines, common in top and bottom panels) and the time histories of the apparent velocity $\tilde{v}_v(t)$ considering the tilt of the sensor. The Imazu-Fukutake G/G_0–γ curves for sand for the average of μ and μ-σ (top) and μ (bottom) were used. The apparent velocity was calculated from the EW (solid green line) and NS (dashed green line) components. The red line shows the summation.

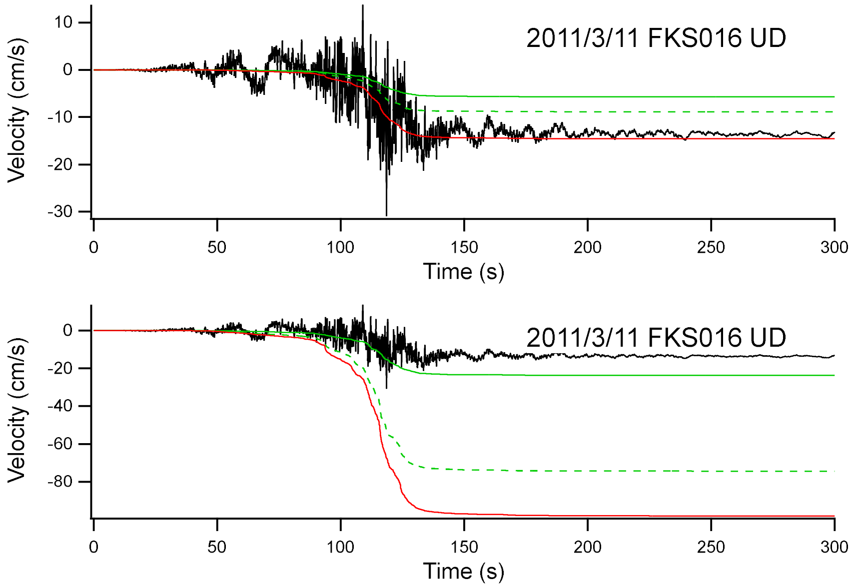

Fig. 10 Velocity waveform obtained by baseline correcting and integrating in time domain the vertical accelerogram of the March 11, 2011, Tohoku earthquake at FKS016 (black lines, common in top and bottom panels) and the time histories of the apparent velocity $\tilde{v}_v(t)$ considering the tilt of the sensor. The Imazu-Fukutake G/G_0–γ curves for clay for the average of μ and μ-σ (top) and μ (bottom) were used. The apparent velocity was calculated from the EW (solid green line) and NS (dashed green line) components. The red line shows the summation.

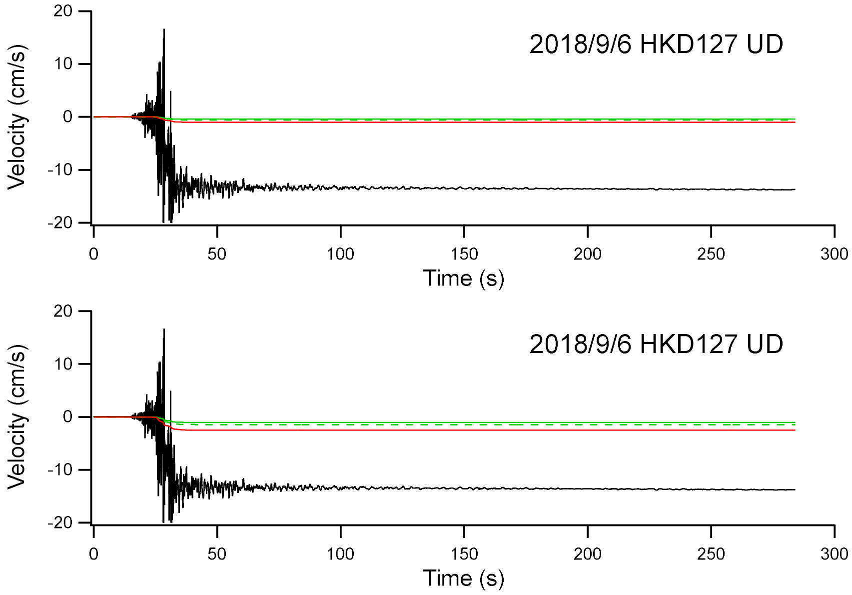

Fig. 11 Velocity waveform obtained by baseline correcting and integrating in time domain the vertical accelerogram of the September 6, 2018, Hokkaido Eastern Iburi earthquake at HKD127 (black lines, common in top and bottom panels) and the time histories of the apparent velocity $\tilde{v}_v(t)$ considering the tilt of the sensor. The Imazu-Fukutake G/G_0–γ curves for sand for μ (top) and μ+σ (bottom) were used. The apparent velocity was calculated from the EW (solid green line) and NS (dashed green line) components. The red line shows the summation.

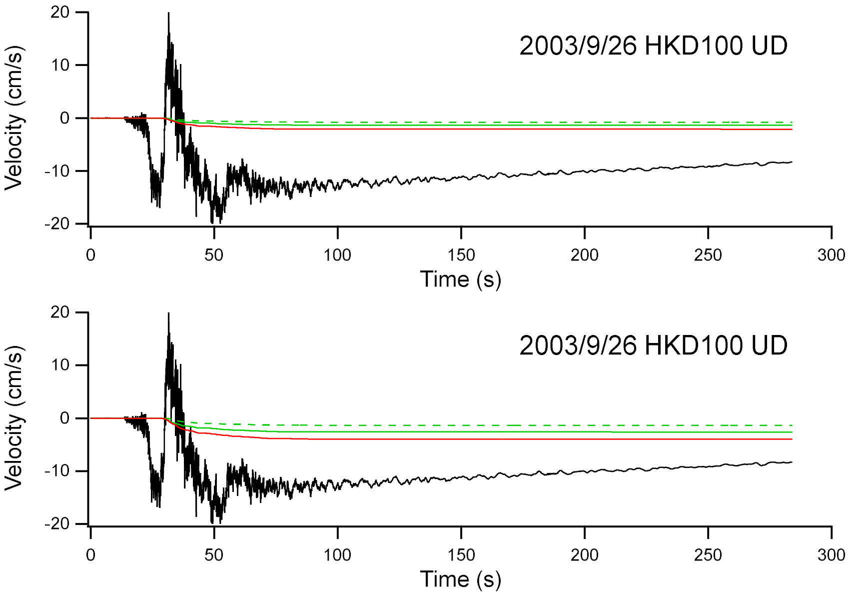

Fig. 12 Velocity waveform obtained by baseline correcting and integrating in time domain the vertical accelerogram of the September 26, 2003, Tokachi-oki earthquake at HKD100 (black lines, common in top and bottom panels) and the time histories of the apparent velocity $\tilde{v}_v(t)$ considering the tilt of the sensor. The Imazu-Fukutake G/G_0–γ curves for clay for μ (top) and μ+σ (bottom) were used. The apparent velocity was calculated from the EW (solid green line) and NS (dashed green line) components. The red line shows the summation.

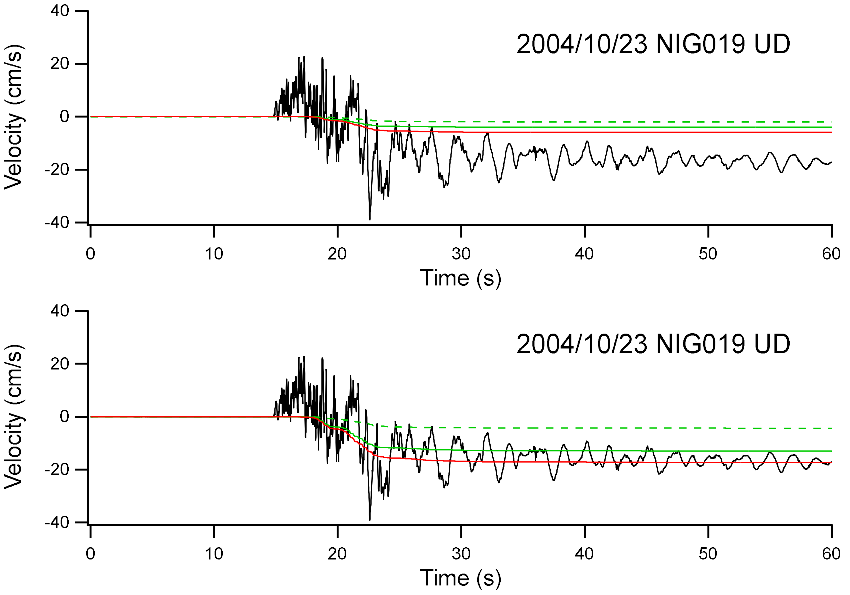

Fig. 13 Velocity waveform obtained by baseline correcting and integrating in time domain the vertical accelerogram of the October 23, 2004, Mid Niigata Prefecture earthquake at NIG019 (black lines, common in top and bottom panels) and the time histories of the apparent velocity $\tilde{v}_v(t)$ considering the tilt of the sensor. The Imazu-Fukutake G/G_0–γ curves for sand for μ (top) and the average of μ and μ+σ (bottom) were used. The apparent velocity was calculated from the EW (solid green line) and NS (dashed green line) components. The red line shows the summation.

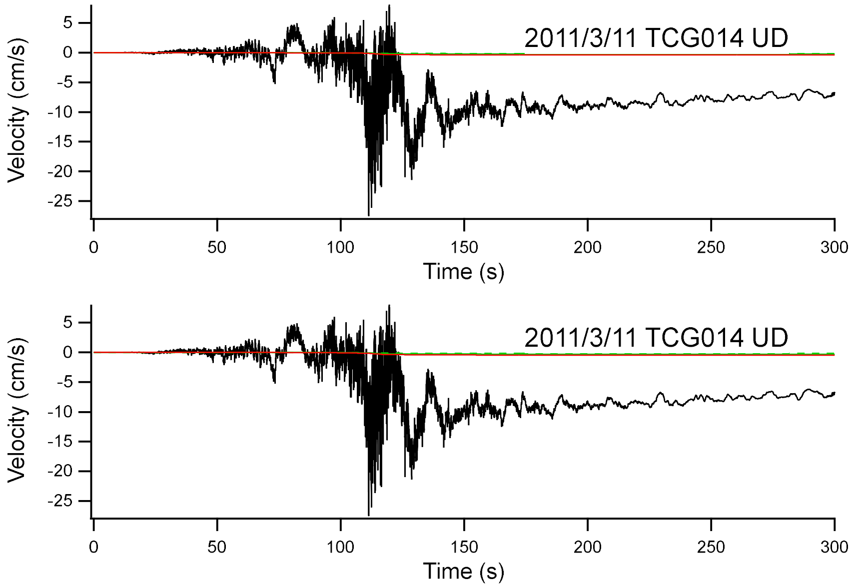

Fig. 14 Velocity waveform obtained by baseline correcting and integrating in time domain the vertical accelerogram of the March 11, 2011, Tohoku earthquake at TCG014 (black lines, common in top and bottom panels) and the time histories of the apparent velocity $\tilde{v}_v(t)$ considering the tilt of the sensor. The Imazu-Fukutake G/G_0–γ curves for clay for μ (top) and μ+σ (bottom) were used. The apparent velocity was calculated from the EW (solid green line) and NS (dashed green line) components. The red line shows the summation.

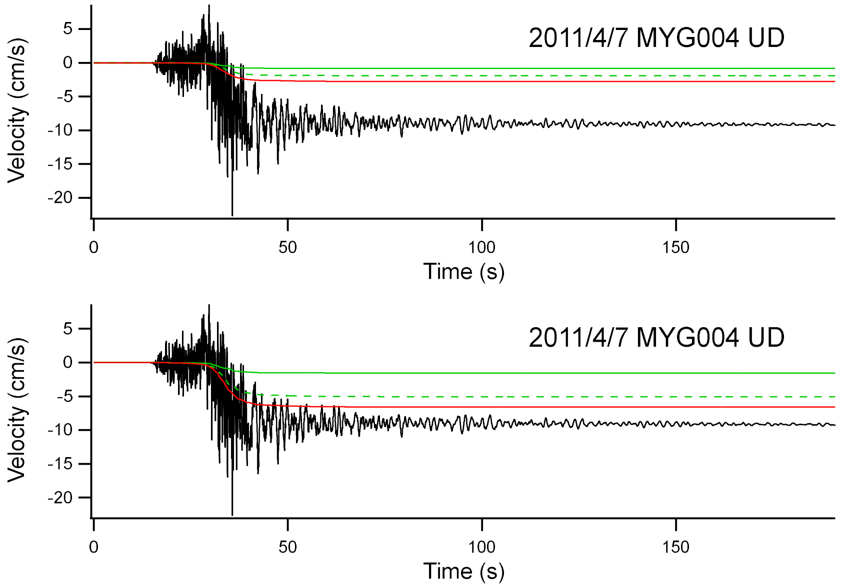

Fig. 15 Velocity waveform obtained by baseline correcting and integrating in time domain the vertical accelerogram of the April 7, 2011, intraslab earthquake at MYG004 (black lines, common in top and bottom panels) and the time histories of the apparent velocity $\tilde{v}_v(t)$ considering the tilt of the sensor. The Imazu-Fukutake G/G_0–γ curves for clay for μ (top) and μ+σ (bottom) were used. The apparent velocity was calculated from the EW (solid green line) and NS (dashed green line) components. The red line shows the summation.

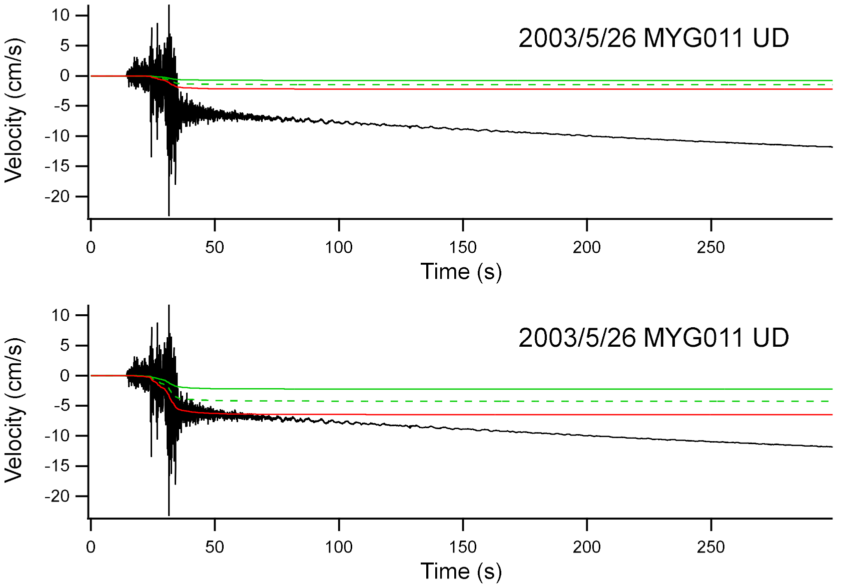

Fig. 16 Velocity waveform obtained by baseline correcting and integrating in time domain the vertical accelerogram of the May 26, 2003, intraslab earthquake at MYG011 (black lines, common in top and bottom panels) and the time histories of the apparent velocity $\tilde{v}_v(t)$ considering the tilt of the sensor. The Imazu-Fukutake G/G_0–γ curves for sand for μ (top) and μ+σ (bottom) were used. The apparent velocity was calculated from the EW (solid green line) and NS (dashed green line) components. The red line shows the summation.

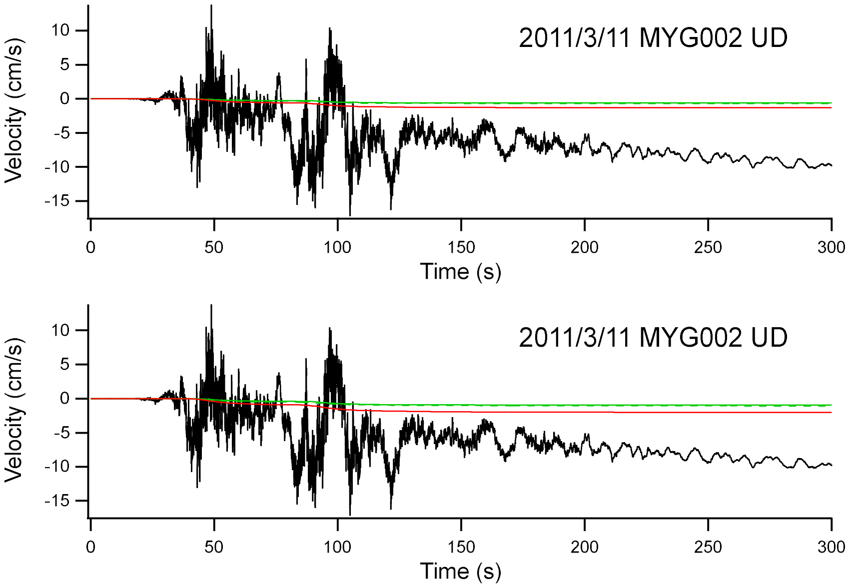

Fig. 17 Velocity waveform obtained by baseline correcting and integrating in time domain the vertical accelerogram of the March 11, 2011, Tohoku earthquake at MYG002 (black lines, common in top and bottom panels) and the time histories of the apparent velocity $\tilde{v}_v(t)$ considering the tilt of the sensor. The Imazu-Fukutake G/G_0–γ curves for sand for μ (top) and μ+σ (bottom) were used. The apparent velocity was calculated from the EW (solid green line) and NS (dashed green line) components. The red line shows the summation.

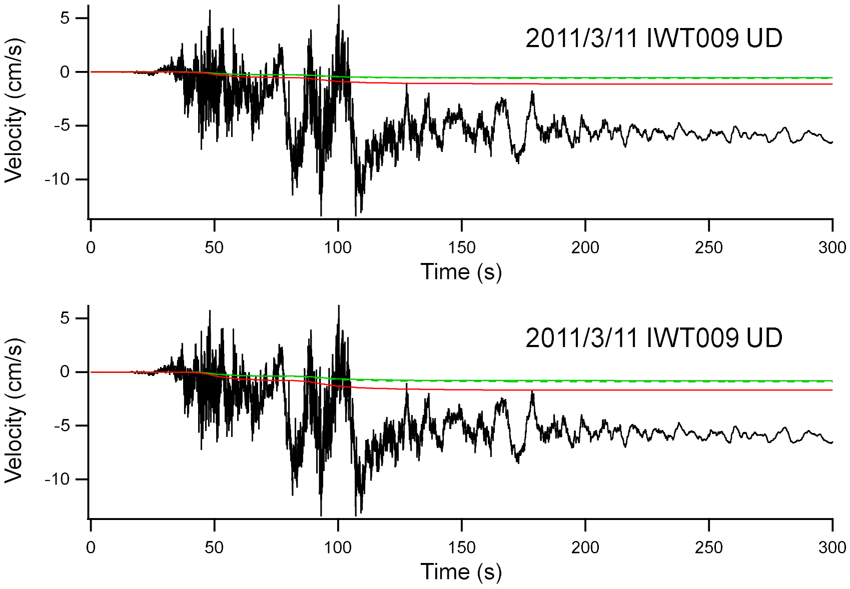

Fig. 18 Velocity waveform obtained by baseline correcting and integrating in time domain the vertical accelerogram of the March 11, 2011, Tohoku earthquake at IWT009 (black lines, common in top and bottom panels) and the time histories of the apparent velocity $\tilde{v}_v(t)$ considering the tilt of the sensor. The Imazu-Fukutake G/G_0–γ curves for sand for μ (top) and μ+σ (bottom) were used. The apparent velocity was calculated from the EW (solid green line) and NS (dashed green line) components. The red line shows the summation.

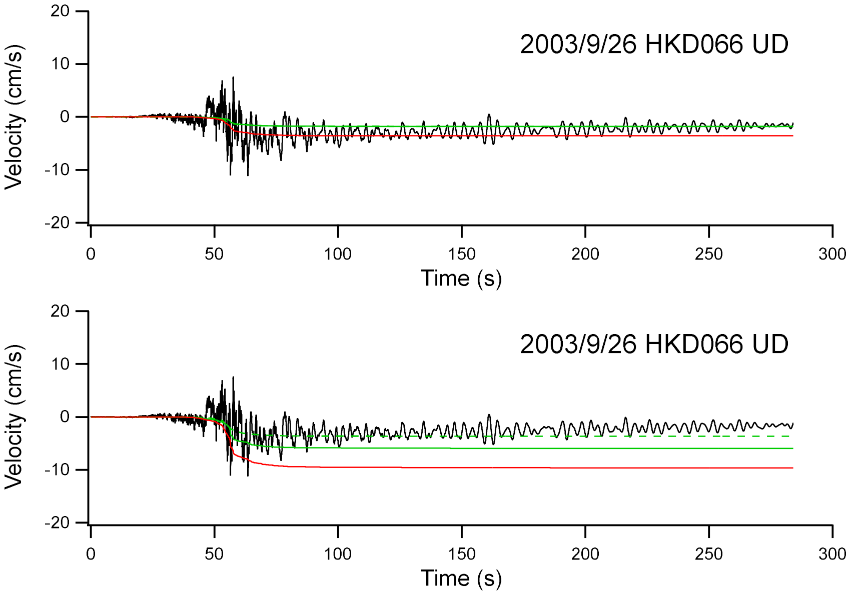

Fig. 19 Velocity waveform obtained by baseline correcting and integrating in time domain the vertical accelerogram of the September 26, 2003, Tokachi-oki earthquake at HKD066 (black lines, common in top and bottom panels) and the time histories of the apparent velocity $\tilde{v}_v(t)$ considering the tilt of the sensor. The Imazu-Fukutake G/G_0–γ curves for sand for μ (top) and the average of μ and μ+σ (bottom) were used. The apparent velocity was calculated from the EW (solid green line) and NS (dashed green line) components. The red line shows the summation.

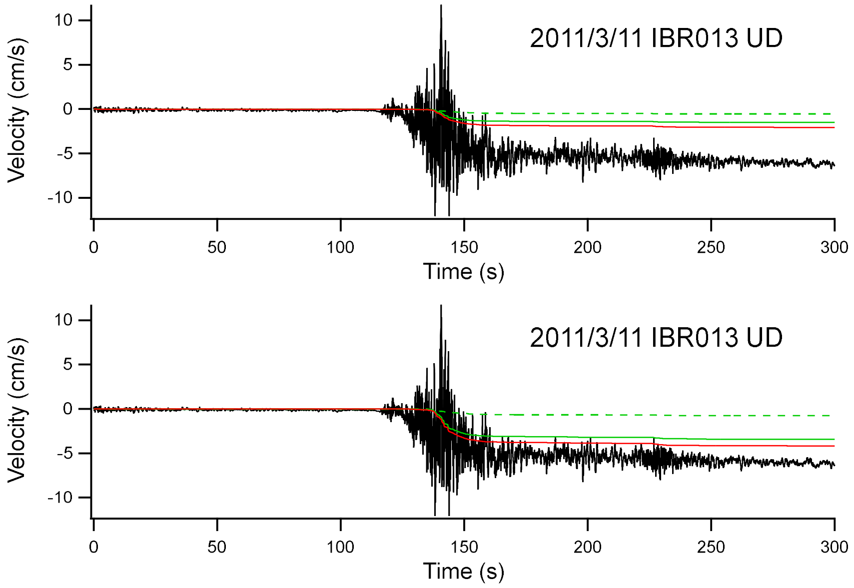

Fig. 20 Velocity waveform obtained by baseline correcting and integrating in time domain the vertical accelerogram of the largest aftershock of the March 11, 2011, Tohoku earthquake at IBR013 (black lines, common in top and bottom panels) and the time histories of the apparent velocity $\tilde{v}_v(t)$ considering the tilt of the sensor. The Imazu-Fukutake G/G_0–γ curves for sand for μ (top) and the average of μ and μ+σ (bottom) were used. The apparent velocity was calculated from the EW (solid green line) and NS (dashed green line) components. The red line shows the summation.

shows the results for the record of the March 11, 2011, Tohoku earthquake at IWT009. The shallowest layer at IWT009 was categorized as fill soil with no further detailed information. If we use the Imazu-Fukutake G/G_0–γ curves for sand, the observed V_{non} value was not successfully reproduced in this case. The possible cause of this result will be discussed later. Figure 19 shows the results for the record of the September 26, 2003, Tokachi-oki earthquake at HKD066. The shallowest layer at HKD066 was categorized as fill soil with no further detailed information. If we use the Imazu-Fukutake G/G_0–γ curves for sand, the observed V_{non} value was successfully reproduced with the curve for μ. Figure 20 shows the results for the record of the largest aftershock of the March 11, 2011, Tohoku earthquake at IBR013. The shallowest layer at IBR013 was categorized as fill soil with no further detailed information. If we use the Imazu-Fukutake G/G_0–γ curves for sand, the observed V_{non} value was successfully reproduced with the curve for the average of μ and μ+σ.

Thus, for 10 out of 16 records listed in Table 1, the observed V_{non} values were successfully reproduced within the possible range of the G/G_0–γ curves ('very good' in Table 2), which shows that the generation mechanism of V_{non} proposed in this study is plausible. However, for the remaining 6 records, the V_{non} values were not successfully reproduced. This point will be discussed in the next section.

5. DISCUSSION

In this section, the possible cause for the unsatisfactory reproduction of the V_{non} values for the 6 records will be discussed.

Because the square of β_0 is involved in the denominator of the right-hand side of Eq. (4), for a small β_0 value, the hyperbola of Eq. (4) is located in the top-right of the G/G_0–γ plane and the intersection of the hyperbola and the G/G_0–γ curve shifts to the right and the G/G_0 value becomes smaller. In the right-hand side of Eq. (7), which is used to calculate the apparent acceleration, not only the square of β_0 but also G/G_0 appears in the denominator, which means that the apparent acceleration is very strongly dependent on β_0. Therefore, possible errors involved in β_0 will result in significant errors in V_{non}. On the other hand, shear wave velocity of the soil is generally dependent on the mean effective stress. As shown in Table 7.4 of Yoshida[10], the shear modulus of sand and clay are often assumed to be proportional to the square root of the mean effective stress. If we assume that the shear modulus is proportional to the nth power of the mean effective stress, the n value ranges from 0.45 to 0.574 for sand for 9 out of 10 documents listed in Table 7.4 and from 0.5 to 0.6 for clay for 4 documents listed in Table 7.4. If the shear modulus is proportional to the square root of the mean effective stress, the shear wave velocity is proportional to the mean effective stress to the power of 1/4. If we assume a ground in which the shear wave velocity β is proportional to the mean effective stress to the power of 1/4 as

$$\beta = \beta_1 (z/z_1)^{1/4} \tag{9}$$

and if we define the averaged shear wave velocity as the thickness divided by the propagation time, the averaged shear wave velocity for a surface layer with a thickness h will be given by

$$\bar{\beta} = h \Big/ \int_0^h \frac{dz}{\beta} = h\beta_1 \Big/ \int_0^h \left(\frac{z}{z_1}\right)^{-1/4} dz = \frac{3\beta_1}{4} \left(\frac{h}{z_1}\right)^{1/4} \tag{10}$$

which is also proportional to the mean effective stress to the power of 1/4.

Then, in the case of HKD127 where the shallowest layer with a shear wave velocity of 130 m/s has a thickness of 2 m, if we interpret the shear wave velocity of 130 m/s as the averaged shear wave velocity for the top 2 m and the real shear wave velocity has a depth dependence, the averaged shear wave velocity for the top 1 m can be reevaluated as 109 m/s. Based on this value and if we use the Imazu-Fukutake G/G_0–γ curves for sand, the observed V_{non} value was reproduced with the curve for μ+σ (Fig. 21). The correction of the shear wave velocity from 130 m/s to 109 m/s, which does not seem significant, greatly improved the results from Figs. 11–21. Similarly, in the case of IWT009, if we reevaluate the averaged shear wave velocity for the top 1 m as 109 m/s and if we use the Imazu-Fukutake G/G_0–γ curves for sand, the observed V_{non} value was reproduced with the curve for μ+σ (Fig. 22). The improvement is significant from Figs. 18–22.

For the rest 4 records, the V_{non} values could not be reproduced even if we consider the depth-dependence of the shear wave velocity. Among these records, for the record of the September 26, 2003, Tokachi-oki earthquake at HKD086, there is no room for correction of the shear wave velocity because the published data suggests the shear wave velocity for the top 1 m of 120 m/s. According to Kinoshita[12], the backfill soil liquefied and the foundation tilted at HKD086 during this earthquake. Kinoshita[12] also estimated the time history of the tilt of the seismometer. The amount of the tilt shown by Kinoshita[12] was equivalent to a ground strain exceeding 5%. On the other hand, the analyses in this study using G/G_0–γ curves (Fig. 6) only yielded a ground strain of 0.2%. In general, when liquefaction occurs, the shear strain of the ground far exceeds the values expected from G/G_0–γ curves. Therefore, it could be reasonable to assume that, at HKD086, the tilt of the sensor was enhanced by the soil liquefaction, resulting in a large V_{non} value.

The remaining three records for which the V_{non} values could not be reproduced are those of the September 26, 2003, Tokachi-oki earthquake at HKD100 and the March 11, 2011, Tohoku earthquake at TCG014 and MYG002. For the MYG002 record, the shallowest layer is a presumably unsaturated sand layer because the compressional wave velocity was less than 1500 m/s. However, excess pore water pressure in the lower layers could have propagated to the shallowest layer resulting in liquefaction of the shallowest layer and a large V_{non} value if we consider the fact that the HKD086 site was liquefied even though the compressional wave velocity for the shallowest layer was less than 1500 m/s. The shallowest layers at HKD100 and TCG014 are presumably unsaturated volcanic clay layers. There are laboratory test data which indicate the generation of excess pore water pressure in unsaturated volcanic clay[13]. At HKD100 and TCG014, the generation of excess pore water pressure could have resulted in

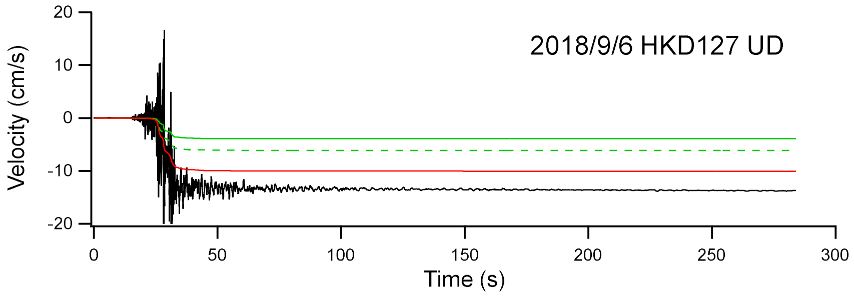

Fig. 21 Time histories of the apparent velocity $\tilde{v}_v(t)$ for the record of the September 6, 2018, Hokkaido Eastern Iburi earthquake at HKD127 assuming the averaged shear wave velocity for the top 1 m of 109 m/s and the Imazu-Fukutake G/G_0–γ curves for sand for μ+σ. The apparent velocity was calculated from the EW (solid green line) and NS (dashed green line) components. The red line shows the summation. The results were compared with the velocity waveform obtained by baseline correcting and integrating in time domain the vertical accelerogram (black line).

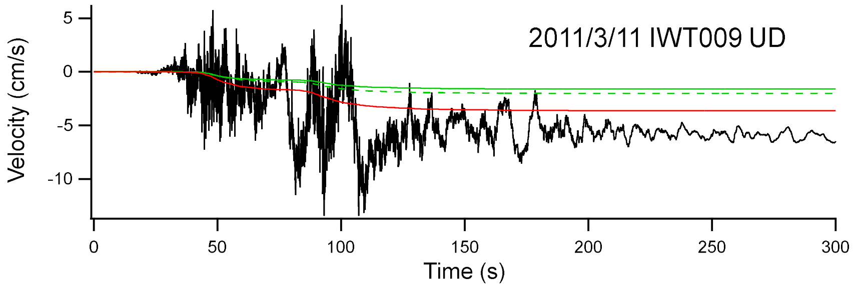

Fig. 22 Time histories of the apparent velocity $\tilde{v}_v(t)$ for the record of the March 11, 2011, Tohoku earthquake at IWT009 assuming the averaged shear wave velocity for the top 1 m of 109 m/s and the Imazu-Fukutake $G/G_0-\gamma$ curves for sand for μ+σ. The apparent velocity was calculated from the EW (solid green line) and NS (dashed green line) components. The red line shows the summation. The results were compared with the velocity waveform obtained by baseline correcting and integrating in time domain the vertical accelerogram (black line).

decrease in shear modulus, increase in shear strain and a large V_{non} value.

As mentioned in 1, in addition to the mechanism proposed in this study in which the horizontal inertia force is partly felt by the vertical sensor, another mechanism can also be considered in which the gravitational acceleration felt by the vertical sensor is tentatively decreased due to the tilt of the sensor. The effect of this mechanism is actually limited as the gravitational acceleration is multiplied by $(1-\cos\theta)$ in this mechanism as pointed out in the previous reports[2), 3)]. In the following, the record of the March 11, 2011, Tohoku earthquake at MYG004 will be analyzed for confirmation purposes. The tilt of the sensor was evaluated for each of the EW and NS components as in Fig. 5, the vector sum was taken, and the time history of the apparent velocity was calculated considering the tentative decrease in the gravitational acceleration felt by the vertical sensor. As shown in Fig. 23, this mechanism cannot reproduce the observed V_{non} value at all.

6. CONCLUSIONS

Paying attention to the reports[1)–3)] that the vertical components of recently-obtained large-amplitude accelerograms often result in a negative residual velocity once they are integrated in time domain, this study investigated the generation mechanism of this negative residual velocity V_{non}. Because the

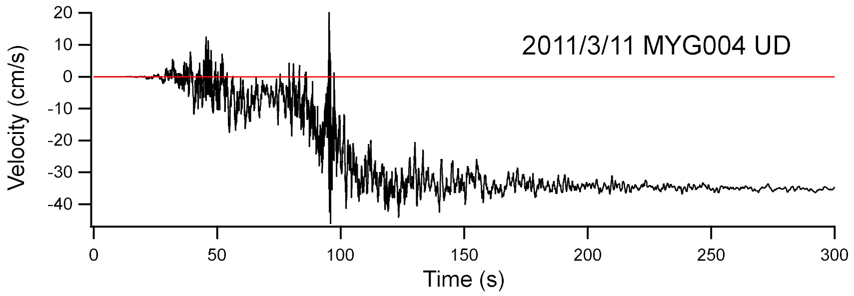

Fig. 23 Time history of the apparent velocity $\tilde{v}_v(t)$ for the record of the March 11, 2011, Tohoku earthquake at MYG004 assuming the Imazu-Fukutake G/G_0–γ curve for clay for the average of μ and μ+σ and considering the tentative decrease in the gravitational acceleration felt by the vertical sensor (red). The result was compared with the velocity waveform obtained by baseline correcting and integrating in time domain the vertical accelerogram (black line).

residual values appear in the velocity waveforms rather than the displacement waveforms, this study was based on a premise that V_{non} is apparent and not representing the actual ground behavior.

One interesting feature of V_{non} is that it is widely observed for various earthquake types, at various hypocentral distances and by various observation networks. This indicates that the mechanism leading to the generation of V_{non} is not a rare special phenomenon but a widely-occurring phenomenon. Another interesting feature of V_{non} is that the residual velocity is always negative. The generation mechanism of V_{non} should also satisfy this condition. This study newly proposed a generation mechanism of V_{non} that satisfies the above two conditions; at the moment of the action of a horizontal inertia force, the sensor is tentatively tilted in that direction and the horizontal inertia force multiplied by $\sin\theta$ is felt by the vertical sensor, where θ is the tilt angle. The tilt of the sensor can be either due to the shear deformation of the ground in the case of a sensor buried in the ground or attached to a foundation which is buried in the ground, or due to the tilt of the house in the case of a sensor installed in a house. This mechanism can be widely-occurring and the apparent residual velocity caused by this mechanism is always negative. In other words, the rocking motion of the sensor or the foundation is the cause of V_{non}.

There are K-NET, KiK-net and JMA records with the V_{non} values exceeding 5 cm/s[3)]. Among the records, the K-NET records were used to investigate whether the proposed mechanism can explain the order of magnitude of the observed V_{non} values, because the sensor foundation is independent from the foundation of the house and the effect of the house is negligible at the K-NET stations. In the analyses, it was assumed that the shear strain in the shallowest layer of the ground determines the tilt of the foundation. The G/G_0–γ curves proposed by Imazu and Fukutake[9), 10)] for various soils were used. As a result, for 12 out of 16 records, the observed V_{non} values were successfully reproduced within the possible range of the G/G_0–γ curves if we consider the depth dependence of the shear wave velocity (Table 2), which shows that the generation mechanism of V_{non} proposed in this study is plausible. The previous reports[1)–3)] suggested the relation between V_{non} and soil dilatancy in which the soil changes its volume under shear. The result of this study does not deny the occurrence of soil dilatancy at the stations where V_{non} was observed. However, the result of this study does indicate that V_{non} can be readily explained by only considering the well-known phenomena such as the decrease of the shear modulus during strong shaking and liquefaction, without considering soil dilatancy.

In this study, 4 records remained for which the V_{non} values could not be reproduced. One of the records is known to have been affected by liquefaction. Therefore, it could be reasonable to assume that the liquefaction resulted in a shear strain far exceeding the values expected from G/G_0–γ curves, resulting in a large V_{non} value for this record. For the other 3 records, liquefaction and the generation of excess pore water pressure could have resulted in a shear strain exceeding the values expected from G/G_0–γ curves, resulting in large V_{non} values. Detailed analysis of this aspect is a subject for future study. In addition, the characteristics of the fill soil after the installation of the station could be different from those in the published borehole data. This remains as a subject for future study, because this study is dependent on published borehole data.

In addition, this study did not consider the sensors installed in houses. According to Aoi et al.[7)], the surface sensors of KiK-net are installed in houses. Even if the sensor is installed in a house, if the tilt of the house is in phase with the action of the horizontal inertia force, the same mechanism as proposed in this study will generate V_{non}. In other words, the rocking motion of the house can cause V_{non}. However, there are two types of house rocking motion, one with tipping and the other without tipping. When the rocking motion accompanies tipping, the tilt of the house and the action of the horizontal inertia force can be out of phase and the generation of V_{non} can be suppressed. If we assume that the sensor is attached to a house and the house rotates about its center of gravity, we can understand that the timing of the tilt of the house and the action of the horizontal inertia force can vary depending on the location of the sensor. Therefore, when the rocking motion accompanies tipping, the generation of V_{non} can be suppressed. In fact, it was found in the previous reports[1)–3)] that V_{non} was not observed for the record at KiK-net IWTH25 during the 2008 Iwate-Miyagi Nairiku earthquake in spite of the large amplitude, although V_{non} was observed at other KiK-net stations. Ohmachi et al.[14)] suggested that house rocking motion with tipping occurred at IWTH25 during the 2008 Iwate-Miyagi Nairiku earthquake. Figure 24 shows the three components of surface accelerograms including the time interval of tipping following Ohmachi et al.[14)]. The positive peak in the vertical acceleration after 19.0 s was interpreted as due to the collision of the house and the ground[14)]. Based on this interpretation, the time interval around 19.0 s with the negative vertical acceleration corresponds to the tipping of the house. In other words, this is the time interval for which the tilt of the sensor is large. For this time interval, the horizontal accelerations are not necessarily large. Thus, it can be concluded that, at IWTH25 during the 2008 Iwate-Miyagi Nairiku earthquake, the tipping of the house resulted in the phase difference of the tilt of the house and the action of the horizontal inertia force and suppressed the generation of V_{non}. In summary, the generation of V_{non} at KiK-net stations should be investigated considering the tipping of the house, based on the information on the size, etc. of the individual houses.

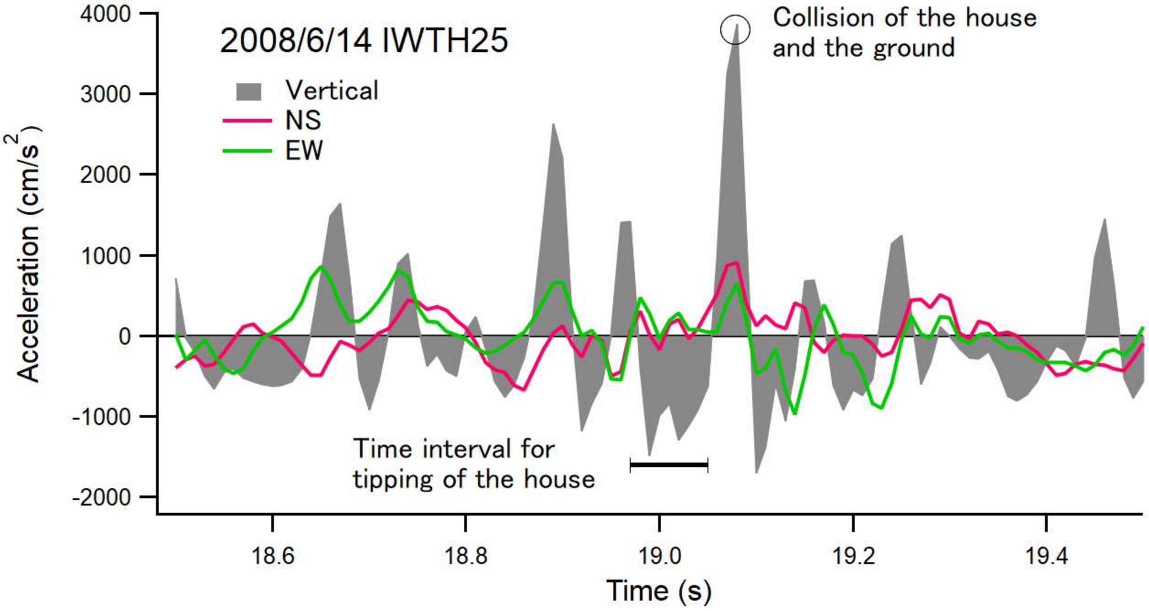

Fig. 24 Three components of surface accelerograms at IWTH25 during the 2008 Iwate-Miyagi Nairiku earthquake

ACKNOWLEDGMENT

The author would like to thank the National Research Institute for Earth Science and Disaster Resilience for K-NET and KiK-net strong motion records.

REFERENCES

1) Satoh, T.: Study on Identification of Nonlinear Site Responses of Vertical Motions Using Strong Motion Records Observed at the Ground Surface, *Journal of Japan Association for Earthquake Engineering*, Vol. 20, No. 2, pp. 17–35, 2020 (in Japanese with English abstract).
2) Satoh, T.: Analysis on Tilt and Settlement in Strong Motion Records, *Journal of Japan Association for Earthquake Engineering*, Vol. 20, No. 7, pp. 69–85, 2020 (in Japanese with English abstract).
3) Satoh, T.: Nonlinear Site Response of Vertical Motions Based on Strong Motion Records, *The 49th Symposium of Earthquake Ground Motion*, Architectural Institute of Japan, Tokyo, Japan, pp. 71–80, 2021 (in Japanese with English abstract).
4) Aoi, S., Asano, Y., Kunugi, T., Kimura, T., Uehira, K., Takahashi, N., Ueda, H., Shiomi, K., Matsumoto, T. and Fujiwara, H.: MOWLAS: NIED Observation Network for Earthquake, Tsunami and Volcano, *Earth, Planets and Space*, Vol. 72, 126, 2020.
5) Loukachev, I., Pralle, N. and Gudehus, G.: Dilatancy-Induced P Waves as Evidence for Nonlinear Soil Behavior, *Bulletin of the Seismological Society of America*, Vol. 92, No. 2, pp. 854–862, 2002.
6) Morio, S., Kato, Y. and Fujii, T.: Elasto-Plasticity Consideration of the Ground on the Large Acceleration Time Histories at Two Earthquakes Observation Sites, *Journal of Japan Association for Earthquake Engineering*, Vol. 17, No. 4, pp. 30–49, 2017 (in Japanese with English abstract).
7) Aoi, S., Kunugi, T. and Fujiwara, H.: Strong-Motion Seismograph Network Operated by NIED: K-NET and KiK-net, *Journal of Japan Association for Earthquake Engineering*, Vol. 4, No. 3, pp. 65–74, 2004.
8) Aoi, S., Kunugi, T., Nakamura, H. and Fujiwara, H.: Deployment of New Strong-Motion Seismographs of K-NET and KiK-net, in Akkar et al. (eds.), *Earthquake Data in Engineering Seismology*, Geotechnical, Geological, and Earthquake Engineering, Vol. 14, pp. 167–186, 2011.
9) Imazu, M. and Fukutake, K.: Dynamic Shear Modulus and Damping of Gravel Materials, *Proceedings of the 21st Japan National Conference on Sol Mechanics and Foundation Engineering*, pp. 509–512, 1986 (in Japanese).
10) Yoshida, N.: *Seismic Ground Response Analysis*, Geotechnical, Geological, and Earthquake Engineering, Vol. 36, 365 pp., 2015.
11) Pillet, R. and Virieux, J.: The Effects of Seismic Rotations on Internal Sensors, *Geophysical Journal International*, Vol. 171, pp. 1314–1323, 2007.
12) Kinoshita, S.: Tilt Measurement Using Broadband Velocity Seismograms, *Bulletin of the Seismological Society of America*, Vol. 98, pp. 1887–1897, 2008.
13) Izutani, S., Kamura, A., Kim, J., Sato. S. and Kazama, M.: Influence of Initial Static Shear and Seismic History on Seismic Shear Behavior of Volcanic Clayey Soil at Residential Area Damaged by the 2016 Kumamoto Earthquake Japan, *Journal of Japan Association for Earthquake Engineering*, Vol. 19, No. 6, pp. 1–15, 2019 (in Japanese with English abstract).
14) Ohmachi, T., Inoue, S., Mizuno, K. and Yamada, M.: Estimated Cause of Extreme Acceleration Records at the KiK-net IWTH25 Station during the 2008 Iwate-Miyagi Nairiku Earthquake, Japan, *Journal of Japan Association for Earthquake Engineering*, Vol. 11, No. 1, pp. 32–47, 2011 (in Japanese with English abstract).

(Original Japanese Paper Published: May, 2023)
(English Version Submitted: May 31, 2025)
(English Version Accepted: July 01, 2025)